Received: 31 August 2021 | Revised: 14 December 2021 | Accepted: 23 December 2021

DOI: 10.1002/cyto.a.24530

TECHNICAL NOTE

MIFlowCyt

ISAC INTERNATIONAL SOCIETY FOR ADVANCEMENT OF CYTOMETRY

CYTOMETRY Journal of Quantitative Cell Science PART A

Development and application of novel BiFC probes for cell sorting based on epigenetic modification

Agnes Mendonca[1] | Oscar Sánchez[1] | Han Zhao[1] | Li Lin[1] | Alan Min[2] | Chongli Yuan[1,3]

[1]Davidson School of Chemical Engineering, Purdue University, West Lafayette, Indiana, USA

[2]Department of Computer Science, Purdue University, West Lafayette, Indiana, USA

[3]Purdue University Center for Cancer Research, West Lafayette, Indiana, USA

Correspondence
Chongli Yuan, Davidson School of Chemical Engineering, 480 Stadium Mall Drive, Purdue University, West Lafayette, IN 47906, USA.
Email: cyuan@purdue.edu

Funding information
National Science Foundation, Grant/Award Numbers: CBET-1512285, CBET-1705560, EF-1935226; Purdue University Center for Cancer Research, NIH, Grant/Award Number: P30 CA023168; Indiana Clinical and Translational Science Institute

Abstract

The epigenetic signature of cancer cells varies with disease progression and drug treatment, necessitating the study of these modifications with single cell resolution over time. The rapid detection and sorting of cells based on their underlying epigenetic modifications by flow cytometry can enable single cell measurement and tracking to understand tumor heterogeneity and progression warranting the development of a live-cell compatible epigenome probes. In this work, we developed epigenetic probes based on bimolecular fluorescence complementation (BiFC) and demonstrated their capabilities in quantifying and sorting cells based on their epigenetic modification contents. The sorted cells are viable and exhibit distinctive responses to chemo-therapy drugs. Notably, subpopulations of MCF7 cells with higher H3K9me3 levels are more likely to develop resistance to Doxorubicin. Subpopulations with higher 5mC levels, on the other hand, tend to be more responsive. Overall, we report for the first time, the application of novel split probes in flow cytometry application and elucidated the potential role of 5mC and H3K9me3 in determining drug responses.

KEYWORDS
breast cancer, DNA methylation, drug resistance, epigenetics

1 | INTRODUCTION

Epigenetic modifications overlying the genome control a host of cellular processes involved in development and differentiation. Common epigenetic modifications include DNA methylation (i.e., methylation at 5-cytosine [5mC]) and various histone post-translational modifications (i.e., methylation and acetylation of lysine and arginine residues). Epigenetic modifications are affiliated with distinctive gene activity (transcription "on" or "off"). For example, 5mC is commonly found in the context of CpG dinucleotides [1] and is responsible for genomic imprinting [2], X chromosome inactivation, and silencing of repetitive elements [3]. Trimethylation of lysine 9 of histone H3 (H3K9me3) is an important repressive mark that is commonly found in gene-poor chromosomal regions and is associated with satellite repeats [4] and retrotransposons [5]. Aberrant changes in epigenetic modifications are commonly observed in various types of cancers, such as leukemia, breast, lung, and colon cancer [6, 7].

Accumulating literature suggests that apart from genetic changes (reviewed in [8]), epigenetics also contribute significantly to cancer initiation and progression [9]. Specifically, the differences in epigenetic modification levels can also partially account for tumor heterogeneity, which may ultimately result in the differential persistence and response of tumor cells to drug treatment [10–13]. The exact connection between epigenetic modifications and drug response/resistance, however, remains elusive since epigenetic variations are innate to cultured cells and it is thus difficult to dissect their contributions due to intrinsic heterogeneity. To address this, we need to sort cells based on their variable epigenetic background, track sorted cell population

Agnes Mendonca and Oscar Sanchez are contributed equally to this work.

via continuous culturing, and subsequently establish the connection between epigenetic modification levels and cell functionality.

Fluorescence assisted cell sorting (FACS) can be applied readily to address the first of these challenges. Antibodies specific to DNA methylation [14, 15] and histone post-translational modifications (PTMs) [16] have been applied to fixed cells and enabled the quantification of epigenetic modifications in cancer cells. For instance, flow cytometry protocols for fixation and antibody staining of H3K27me3 and H3K9me3 were developed by Watson et al. [16] and were used to assay these modification levels in clinical samples from leukemia patients. These studies confirmed that epigenetic heterogeneity is a common observation in tumor samples, but are limited to applications in fixed cells. Specifically, fixation (for all modifications) and denaturation step (specific for 5mC) can alter cellular morphology. When identifying repressive modifications present in condensed chromatin, epitope masking (loss of binding sites due to lack of accessibility) can be a very significant concern [17]. Most importantly, antibody-based sorting approaches, are limited to fixed cells and thus precludes dynamic tracking of the sorted cell population. To the best of our knowledge, there are no live-cell compatible epigenetic sorting tools.

The limitations of using antibodies to track epigenetic modifications over time, extends to other platforms such as microscopy, as well. Recently, a few tools have been developed to overcome these limitations, such as live cell compatible Fab based probes [18, 19], fluorescent-protein fusions [20–22], (Förster resonance energy transfer) FRET-based [23] and (bimolecular fluorescence complementation) BiFC-based [24] approaches. Specifically, fluorescent labeled antigen binding fragments (Fab) have been used to track H3K9me3 and H3K27ac in live mouse embryo imaging [18]. The method can be extended to study other histone PTM levels but requires the development and characterization of highly specific monoclonal antibody fragments. The binding duration and affinity of the Fab probes can also affect the readout of the dynamic change in modification levels. Similarly, genetically encoded antibody based "mintbodies" have been generated to track H4K20me1 [25] in mammalian and yeast cells. Engineered epigenetic "reader" domains have been emerging as a promising candidate for probing epigenome changes in situ due to their high selectivity. For instance, the methyl binding domain (MBD) from MBD1 has been used to monitor changes in DNA methylation (5mC) in mouse embryonic stem cells [26, 27]. These probes have also been used in combinations to trace nucleosomes with distinctive combinations of epigenetic modifications [20]. Furthermore, epigenetic reader domains have been coupled with advanced fluorescent techniques, such as FRET and BiFC for improved signal-to-noise ratio. For example, FRET based sensors have been developed using the chromodomain from the heterochromatin protein 1 (HP1) and Polycomb (Pc) for detecting H3K9me3 [28] and H3K27me3 [29], respectively. Bromodomain has also been used to detect histone acetylation such as H4K5/8/12 ac [30, 31]. FRET interactions occur between donor and acceptor moieties which are connected by an epigenetic reader domain and its targeted histone sequence. The FRET-sensor can be used to quantify the modification level of the "reporter" histone but does not directly inform the modification level of endogenous histones. BiFC probes have also been developed recently to monitor sequence-specific changes in living cells and can be used to modular cellular response to epigenetic drugs and editing tools [24]. The probes in this work offer better signal-to-noise ratio compared to other sensors, but have not been optimized individually for binding affinity offering potential room for improvement.

Previous work from our group and others have shown that utilization of tandem repeats, for example adjacent repeats of the same epigenetic "reader" domain, can enhance the target recognition by improving its selectivity and affinity [21, 22, 27, 32, 33]. Built upon this, we have refined engineered probes in this work by generating tandem repeats of native "reader" domains that recognize specific epigenetic modifications, namely 5mC and H3K9me3 because of their significant roles in cancer progression and disease development. BiFC was adopted to enhance the signal-to-noise ratio. We demonstrated the use of these probes to sort cells based on their 5mC or H3K9me3 levels. Lastly, the contribution of epigenetic heterogeneity to drug resistance and tumor formation was assessed using a breast cancer cell line (MCF7). In this work, we demonstrated the proof-of-concept application using immortalized human cell lines. We anticipate the technology to be adaptable for primary patient cells after establishing optimal delivery strategies via either viral packaging, liposome assisted transfection or electroporation.

2 | MATERIALS AND METHODS

2.1 | Design and validation of epigenetic probes

H3K9me3 is typically recognized with high selectivity by the chromodomain of HP1 [34] and CDY family of proteins [35]. The affinity of chromodomain of human CDY1 ($K_D \sim 0.5 \pm 0.1$ μM) [35, 36] was found to be higher than those of human HP1α (K_D 13 ± 3 μM) [37] and HP1β (K_D 3 ± 1 μM) [37]. 5mC detection via methyl binding domains (MBDs) of MBD1 was well-documented in literature [38–40]. We thus chose the chromodomain of human CDY1 and methyl-binding domain of MBD1 as the H3K9me3 and 5mC "reader" domains, respectively, for this study. We adopted a tandem repeat strategy similar as described in literature [21, 22, 27, 32, 33] to improve the performance of our engineered probes. Epigenetic probes consisting of both monomeric (one repeat unit of the "reader" domain, and referred to as "monomeric" probe later on) and dimeric (two adjacent repeat units of the "reader" domains linked by a flexible linker, and referred to as "dimeric" probe later on) fused to a fluorescent protein (e.g., mEGFP) were constructed and compared. The optimized in situ probes were subcloned into a PRK5 plasmid, while for in vitro validation assays a bacterial expression vector was constructed using a pET21b vector.

Optimal BiFC epigenetic probes, hereafter referred to as split-probes, compatible with sorting applications were designed as illustrated in Figure 1A with a detection mechanism outlined in Figure 1B. The amino acid sequences of the "reader" domains are shown in Table S1 (Supporting Information). Negative controls were

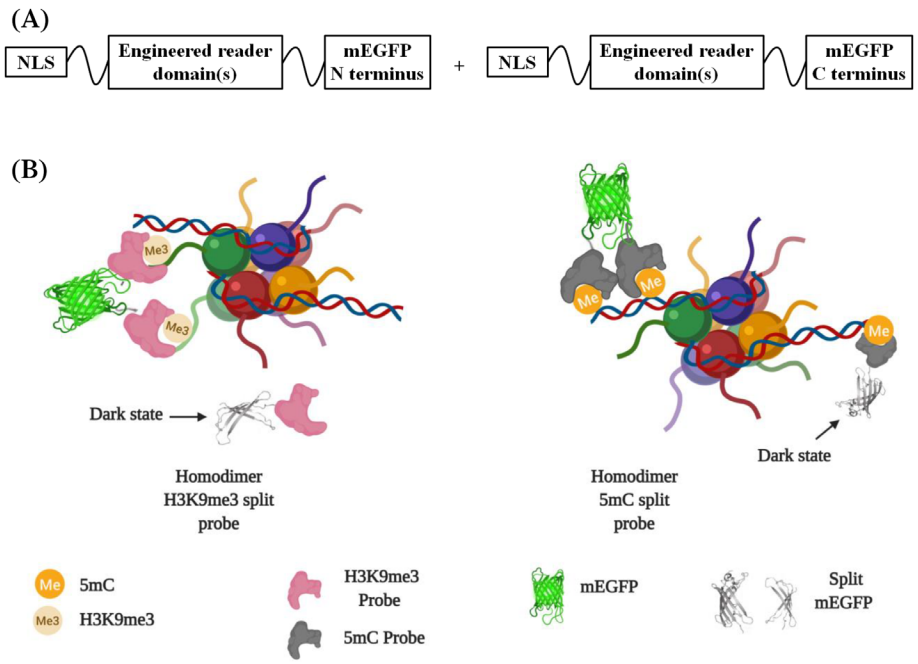

FIGURE 1 (A) A schematic illustration of probe design. Each probe pair contains two probes with an engineered reader domain flanked by a nuclear localization signal (NLS) and a split fluorescence protein (mEGFP N- or C- terminus), respectively. A flexible G4S liner was used to connect each functional domain. (B) Illustration of the detection mechanism utilized by our BiFC probe pair. In a genomic locus enriched in the modification of interest, that is, DNA methylation (right) or H3K9me3 (left), the two probes within a probe pair are expected to bind in a close vicinity, dimerize and fluoresce based on bimolecular fluorescence complementation (BiFC) [Color figure can be viewed at wileyonlinelibrary.com]

constructed like the full-length or BiFC probes but without the engineered "reader" domain.

2.2 | Mammalian cell culture, transient transfection, and drug treatments

Human embryonic kidney (HEK) 293T cells were selected as the proof-of-concept platform for the engineered probes due to their ease in maintenance and transfection [41]; while MCF7 luminal breast tumor cell lines were selected as the application platform for the engineered probes since they are known to develop drug-resistance after prolonged treatments [42, 43]. HEK293T and MCF7 cells (ATCC) were cultured and maintained in DMEM (Dulbecco's modification of Eagle's Medium) supplemented with 10% (v/v) fetal bovine serum (Atlanta Biologicals) and 1% (v/v) of Penicillin–Streptomycin solution (Gibco, Grand Island, NY) in an atmosphere of 5% CO_2 at 37°C. Cells were grown in 100 mm tissue culture treated plates (Corning, Corning, NY) and passaged every 2–4 days after reaching a confluency of ~80% following standard cell culture protocols [44]. For microscopy-based analysis, cells were seeded onto ibidi 8 well μ slides (ibidi USA, Fitchburg, WI).

Lipofectamine 3000 (Life Technologies, Carlsbad, CA) was used as the transfection reagent to transiently transfect cells with plasmids encoding the probe, following manufacturer's protocols. Transfected cells were detached from the surface using TrypLE (~24 h post-transfection) and resuspended in PBS, pH 7.4 with 1% BSA prior to FACS sorting. For culturing cells on Matrigel (Catalog#356230, Lot# 6095004, Corning, Bedford, MA), 12 well plates were coated with 50 μl of Matrigel and cells were seeded on to the solid gel.

Epigenetic drugs were used to perturb cellular epigenetic modification levels. Specifically, BIX-01294 (Sigma, St. Loius, MO) a histone methyltransferase (G9a HMTase) inhibitor was used to lower the H3K9me3 levels. The drug concentrations chosen for BIX-01294 treatment were 3 and 5 μM, respectively, in order to minimize toxicity effects on cells [45]. A DNMT1 inhibitor, RG108 was used at a concentration ranging from 10 to 100 μM to lower the DNA CpG methylation level [46, 47]. Epigenetic drugs were directly spiked into cell culture media. Similarly, doxorubicin exposure was performed at varying concentrations from 0 to 22 μM to assess the cytotoxic effects of this drug on MCF7 cells. All cells were exposed to drugs for a minimum of 48 h prior to analysis.

2.3 | Fluorescence assisted cell sorting (FACS)

All flow cytometry data were collected using a BD FACS Aria (Becton Dickson, San Jose, CA) with a 488 nm laser line and a 530/30 nm FITC filter. Un-transfected HEK293T cells were used to determine the proper gating used in the analysis (see Figure S1 (Supporting Information)). All cytometry data was analyzed using FCS Express software (De Novo software, Glendale, CA).

Cell sorting was performed using a BD FACS Aria III Cell sorter (Becton Dickson, San Jose, CA). The sorter is equipped with temperature control and a biosafety cabinet to ensure sterility of the cell samples pre- and post- sorting. Similar gating strategy as described above was used. Raw data were deposited on Flow Repository and are accessible via the ID: FR-FCM-Z4MF.

2.4 | Immuno-staining

Transfected cells can be fixed and then immune-stained with commercial antibodies using an established protocol with some modifications

[48]. Specifically, cells transfected with either the H3K9me3 or the 5mC probes were fixed and permeabilized using cold methanol for 10 min [49]. Cells were then blocked with 1% BSA in PBS for 1 h followed by incubation with primary antibody for 1 h at room temperature. For 5mC antibody staining, additional denaturating and neutralization steps were introduced by incubating fixed cells with 4 N HCl for 30 min followed by a neutralization step with 100 mM Tris–HCl (pH 8.5) and three times PBS washes. This step is essential, since commercial 5-mC antibodies only bind to single-stranded DNA [50]. After incubation with primary antibodies, cells were then washed with PBS three times and incubated for 1 h at RT with the secondary antibody. Cells were then washed with PBS three times and stored at 4°C before imaging. Commercial antibodies anti-H3K9me3 (ab8898, Abcam, MA) + Goat-anti-rabbit, Alexa Fluor 568 (ab175471, Abcam, MA), and anti-5Mc (#61480, Active motif, CA) + Donkey-anti-mouse Alexa Fluor 647 (a31571, Invitrogen, CA) were used in the validation for H3K9me3 and 5mC, respectively.

2.5 | Microscopy imaging

Cell imaging was performed on a Nikon Eclipse Ti-C1 microscope equipped with a 60× oil immersion objective lens, 488 and 647 nm laser lines, and automated stage. Z-stack images of cells were collected and compiled using Nikon EZ-C1 software.

2.6 | Quantifying cellular epigenetic levels using ELISA

ELISA assay kits were used to assess the global epigenetic changes in cell population. Genomic DNA was extracted using a Genomic DNA Extraction kit (Invitrogen). Histones were extracted following an acid extraction procedure. The Global DNA methylation kit (cat #55017, Active Motif, Carlsbad, CA), H3K9me3 ELISA (cat #53109, Active Motif, Carlsbad, CA) and total histone H3 (cat #53110, Active Motif, CA) ELISA kits were used to assay the DNA methylation, H3K9me3 and histone H3 levels, respectively.

2.7 | Bio-layer interferometry

To assess the specificity of the dimeric H3K9me3 probe, we used bio-layer interferometry (BLI, OctetRed 384, ForteBio, Menlo Park, CA). The non-fluorescence labeled probe was expressed in bacteria and purified as described in our previous works [21, 22]. Biotinylated histone peptides (with sequence detailed in Table S2) were loaded on streptavidin-activated capture biosensors (ForteBio, Menlo Park, CA). A binding buffer (25 mM Tris–HCl, 25 mM, pH 7.2; NaH_2PO_4, 25 mM, pH 7.2; NaCl, 25 mM; EDTA, 1 mM; DTT, 1 mM; BSA, 0.1% $^{W}/_{V}$; and Tween 20, 0.05%$^{V}/_{V}$) was used to perform all binding assays.

2.8 | Cell viability assay

Doxorubicin toxicity over sorted MCF7 cells via H3K9me3 or 5mC background was evaluated by monitoring different parameters such as cell proliferation, cell viability and apoptosis. Cell viability was assessed using a commercial MTT kit (cat#ab211091, Abcam, US) according to the manufacturer's recommendations.

2.9 | Data analysis and statistics

ImageJ (NIH, MD) plugin JACoP was used to determine the co-localization of probe-transfected and immuno-stained images. Fluorescence intensity per nuclei (FIPN) were determined via a customized pipeline written using Cellprofiler (Broad Institute, MA). For all image analysis, more than 100 cells were analyzed from at least three independent replicates. All ELISA experiments were carried out using at least three biologically independent replicates. FCS Express software (De Novo software, Glendale, CA) was used to generate the intensity histograms from FACS. Data collected for this study is available in MIFlowCyt (Supporting Information).

All statistical analysis and error propagation calculations were performed using GraphPad Prism. Pair-wise comparison was performed using ANOVA followed by *post-hoc* Tukey's test, $^{*}p = 0.05$ is considered statistically significant unless otherwise stated. OriginPro and GraphPad Prism were used for creating figures and graphs. Principal component analysis (PCA) and k-means clustering analysis were performed using RStudio (version 1.0.143). The base R function prcomp was used to scale and center the variables and run the PCA while *k*-means was used to perform k-means clustering analysis.

3 | RESULTS AND DISCUSSION

3.1 | Optimization and validation of epigenetic recognition motifs in situ

We started by screening different designs of recognition motifs for maximal similarity to antibody staining using a recognition motif fused to a fluorescent protein (mEGFP) (see Figure S2A (Supporting Information)). The "reader" domains were selected based on chromodomain of the human CDY family of proteins [35] and the methyl binding domain (MBD) of the human MBD1 [21, 51, 52] for probing H3K9me3 and 5mC, respectively. We first compared the performance of our monomeric and dimeric epigenetic probes following our established protocol [21, 22, 53]. The dimeric H3K9me3 and 5mC probes exhibit increased numbers of puncta after transfected into HEK293T cells suggesting increased sensitivity as shown in Figure S2B–C (Supporting Information).

Although the chromodomain of CDY1 has been shown to bind specifically to H3K9me3 [35], it has not been used previously as an in situ probe for H3K9me3 warranting further characterization. Cells

transfected with monomeric or dimeric H3K9me3 probes were shown in Figure 2A and Figure S3 (Supporting Information). The transfected cells exhibit the expected binding patterns with a rim of H3K9me3 enriched at the nuclear periphery and large islands of H3K9me3 corresponding to peri-nucleolar heterochromatin [54]. These cells were then stained with H3K9me3 antibodies followed by co-localization analysis using Mander's correlation analysis as shown in Figure 2B and Figure S3 (Supporting Information). Both monomeric and dimeric H3K9me3 probes have a good resemblance in the pattern and distribution of the observed foci compared with immuno-stained cells. Pixel-by-pixel co-localization analysis revealed that the Mander's Colocalization Coefficients (MCCs), M1 and M2, for the dimeric H3K9me3 probes (M1 = 0.96 ± 0.05 and M2 = 0.94 ± 0.08) are significantly higher than the ones obtained for the monomeric H3K9me3 probes (M1 = 0.92 ± 0.10 and M2 = 0.91 ± 0.08) with $p < 0.01$ (see Figure S3B (Supporting Information)). Dimeric H3K9me3 probes were thus selected for in vitro characterization via BLI. To do that, the dimeric probe was subcloned into a pET vector and expressed recombinantly following our reported protocol to determine the binding affinity and selectivity [21, 22]. The affinity measurements were performed using Bio-Layer Interferometry against wild-type H3, H3K9me2, and H3K9me3 peptides (sequences detailed in Table S2 (Supporting Information)). The recombinant dimeric chromodomains (see Figure S4A for expression (Supporting Information)) used in constructing our H3K9me3 probes were found to be highly specific for H3K9me3 compared to wild-type H3 or H3K9me2 peptides (Figure S4B (Supporting Information)). The binding affinity of the selected H3K9me3 recognition domains to H3K9me3 peptides were

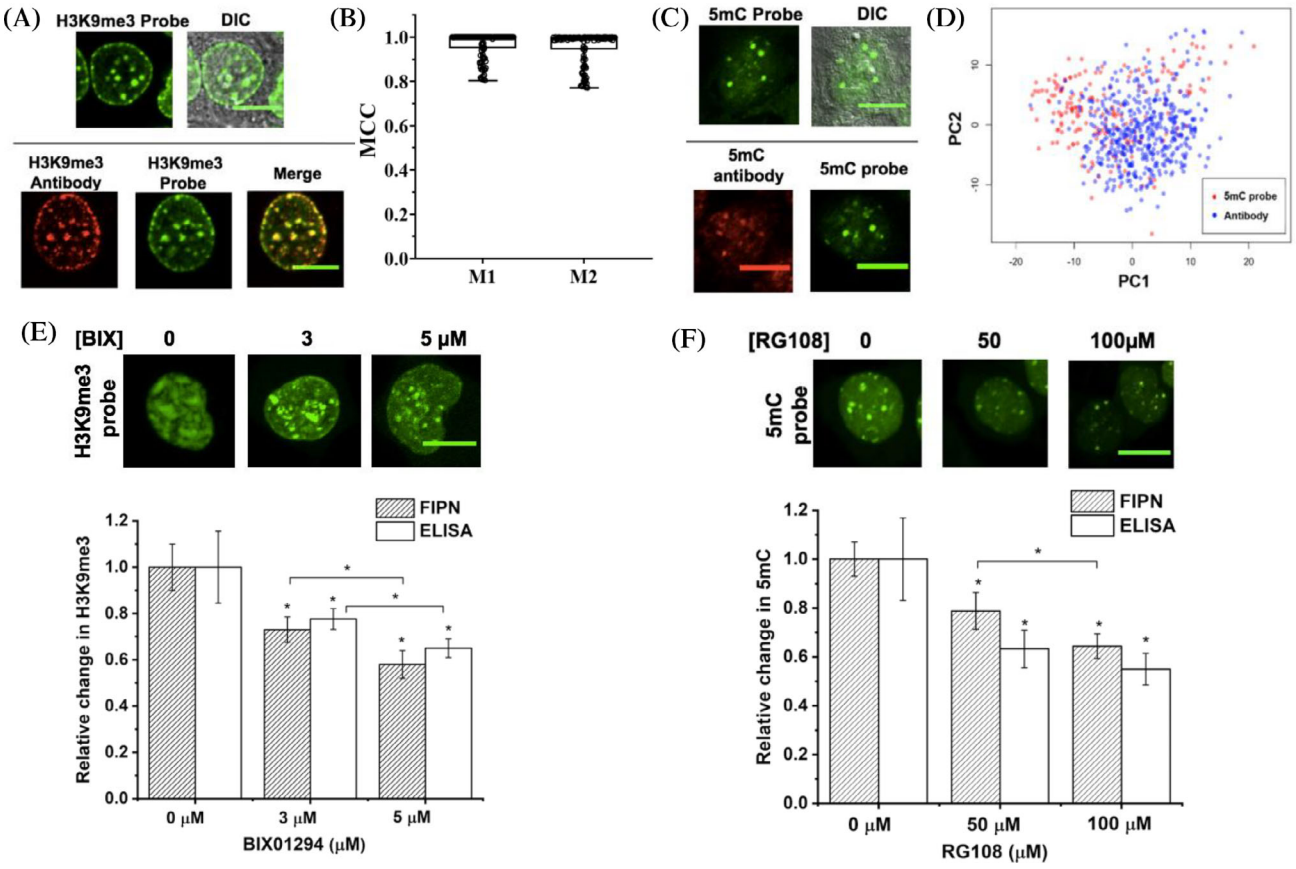

FIGURE 2 (A) *Top panel*: 2D confocal image slices of live HEK293T cells transfected with the H3K9me3 probe. *Bottom panel*: Representative 2D confocal image slices of the binding pattern of the H3K9me3 probe with commercial anti-H3K9me3 antibody shows perfect co-localization. (B) The Mander's correlation coefficients (MCC), M1 and M2 for the H3K9me3 probe and counterstained commercial H3K9me3 antibody are close to 1 indicating a high degree of positive correlation. M1 = 0.92 ± 0.1 and M2 = 0.94 ± 0.1. The data is obtained from $n = 100$ cells. (C) *Top panel*: 2D confocal image slices of live HEK293T cells expressing the 5mC probes and showing the characteristic pattern of DNA methylation. *Bottom panel*: Anti-5mC antibodies and the 5mC probes have similar binding patterns (note that these 2D confocal image slices are not from the same cell). (D) PCA of the binding pattern of the 5mC probe and commercial 5mC antibodies suggests that they are not statistically different from one another. (E) BIX01294 was used to lower the H3K9me3 levels and the change was captured by the H3K9me3 probes. Top: Typical 2D projection of z-stacks of BIX01294 treated cells. ELISA for H3K9me3 was conducted to verify the decrease in H3K9me3 levels. (F) Decrease in DNA methylation level induced by RG108 was captured by the 5mC probe as quantified by the decrease in FIPN. Top: Typical 2D projection of z-stacks of RG108 treated cells. An ELISA based approach was used to validate the activity of RG108 in HEK293T cells. Data represents $n = 100$ cells for microscopy based analysis and $n = 4$ for ELISA; error bars represent standard deviations. * Indicates a statistically significant difference between samples at a $p < 0.05$ and was calculated by a one-way ANOVA analysis followed by Tukey's post-hoc test. Scale bar = 10 μm [Color figure can be viewed at wileyonlinelibrary.com]

found to be ~0.16 ± 0.02 μM. Compared to other chromodomains such as chromodomains from *Drosophila* HP1a (K_D = 0.24 ± 0.02 μM for a dimeric construct [22]), the selected chromodomain is slightly advantageous by having a higher affinity.

Previous work including our own has demonstrated the feasibility of using MBD of the human MBD1 protein to probe CpG methylation in vitro and in situ [26, 27, 51]. The utilization of tandem repeats of MBD was also demonstrated to improve the binding affinity to 5mC in literature [27]. We adopted a similar design in this work with the sequence of "reader" domain detailed in Table S1 (Supporting Information). To confirm that a dimeric domain has higher affinity than the monomeric one, we expressed the monomeric and dimeric MBD proteins recombinantly and carried out DNA-binding assays as shown in Figure S5 (Supporting Information). At equivalent DNA: protein ratios, dimeric MBD domains form more DNA-protein complex as slow-moving bands on native PAGE suggesting higher affinity to methylated DNA. Typical images of cells transfected with the 5mC probes in either a monomeric or dimeric form are shown in Figure S2B (right, Supporting Information). The recognition motif containing dimeric repeats of "reader" domains exhibit similar patterns to immuno-stained cells with small bright foci of varying sizes inside nuclei (see also Figure 2C) consistent with literature observations [27, 55]. We thus chose the dimeric MBD domain as our engineered reader domain for 5mC probes and carried out further validation.

We attempted co-staining followed by co-localization strategy to validate our 5mC probes as before. This strategy, however, did not work well for 5mC probes potentially due to the cellular distortions during the DNA denaturation step essential for applying 5mC antibodies that only bind to single-stranded DNA. To compare the pattern between transfected and immuno-stained cells, we collected a large number of cell images (n > 100), extracted and quantified pattern features using an approach outlined in our previous work [56] and performed a PCA between these two cell populations as shown in Figure 2D. k-means clustering analysis was carried out to determine the number of distinctive clusters based on their imaging features and suggest that cells transfected with our optimized 5mC probes and immunostained belong to the same cluster. We thus concluded that cells transfected with our dimeric 5mC probe and immuno-stained are essentially indistinguishable in between, suggesting a similar pattern matching.

Collectively, we have determined that recognition motifs composed of dimeric reader domains exhibit high affinity for their specific epigenetic target, can be transfected into cells, and exhibit almost identical patterns to cells stained with commercial antibodies, validating their suitability for probing epigenetic features. We further determined the accuracy of the selected recognition motifs in quantifying changes in H3K9me3 and 5mC induced by small-molecule inhibitors of epigenetic enzymes, namely BIX01294 and RG108 for inhibiting histone methyltransferase G9a and DNMT1, respectively. The treatment concentrations of [BIX01294] = 3 and 5 μM and [RG108] = 50 and 100 μM were chosen to induce significant changes in the modification levels while keeping cell viability and phenotypic features intact based on existing literature [47, 57]. All cells were treated for a minimum of 48 h before imaging or harvested for ELISA. Typical images of cells under different treatment conditions can be found in Figure 2E–F (top) with more images shown in Figure S6 (Supporting Information). After BIX treatment, H3K9me3 probes exhibit smaller puncta features inside cells. RG108 treatment seems to significantly reduce the number of puncta inside nucleus. The fluorescence intensity per nuclei (FIPN) is typically used to quantify signals generated from probes [58] and thus determined for cells under different treatments. Percentage changes in FIPN responding to inhibitor concentrations were compared to percentage changes in epigenetic modifications determined via ELISA as shown in Figure 2E–F (bottom). FIPN decreases with increasing BIX01294 or RG108 concentrations. A strong positive correlation was observed between FIPN and ELISA reading suggesting that our dimeric probes can quantify changes in epigenetic modifications via FIPN. The observed changes in H3K9me3 FIPN under varying BIX01294 concentrations are also consistent with changes in H3K9me3 measured via Western blot as shown in our previous work via a different H3K9me3 probe design [22]. We thus concluded that our optimized epigenetic recognition motif can quantify changes in the selected modification with a comparable accuracy to commercial ELISA kit.

3.2 | Analysis and sorting of cells based on their epigenetic modification level via BiFC pair of epigenetic probes

Built-upon the optimized epigenetic recognition motif, we constructed a BiFC pair of epigenetic probes (see Figure 1A) and demonstrated their applications in flow cytometry. The applications of similarly designed BiFC pairs in fluorescent microscopy have been demonstrated previously in literature [24]. We hence focused on the FACS application here. Compared to fluorescent fusion probes, BiFC strategy relies on fluorescence complementation between two fragments as shown in Figure 1B. Since individual N- or C- terminal fragments are non-fluorescent, signal is only obtained when the two halves are in close proximity and thus offering significantly improved signal-to-noise ratio as extensively demonstrated in literature [24, 59, 60]. Probes employing the BiFC strategy are henceforth referred to as H3K9me3 or 5mC split-probes. Typical images of cells transfected with H3K9me3 and 5mC split-probes can be found in Figure S7 (Supporting Information) showing a similar pattern as observed in immuno-stained cells.

We then sorted cells transfected with H3K9me3 or 5mC split-probe and treated with varying epigenetic inhibitors. BIX01294 and RG108 are found effective in reducing H3K9me3 and 5mC levels, respectively, and thus used to induce distinctive epigenetic modification levels in cells. These cells were then analyzed using FACS to generate intensity histograms as shown in Figure 3A and B. Median fluorescent intensity (MFI) was also determined from the histogram and used to quantify average changes in fluorescence intensity corresponding to epigenetic changes. Relative changes in MFI are compared to changes in epigenetic modification level as determined

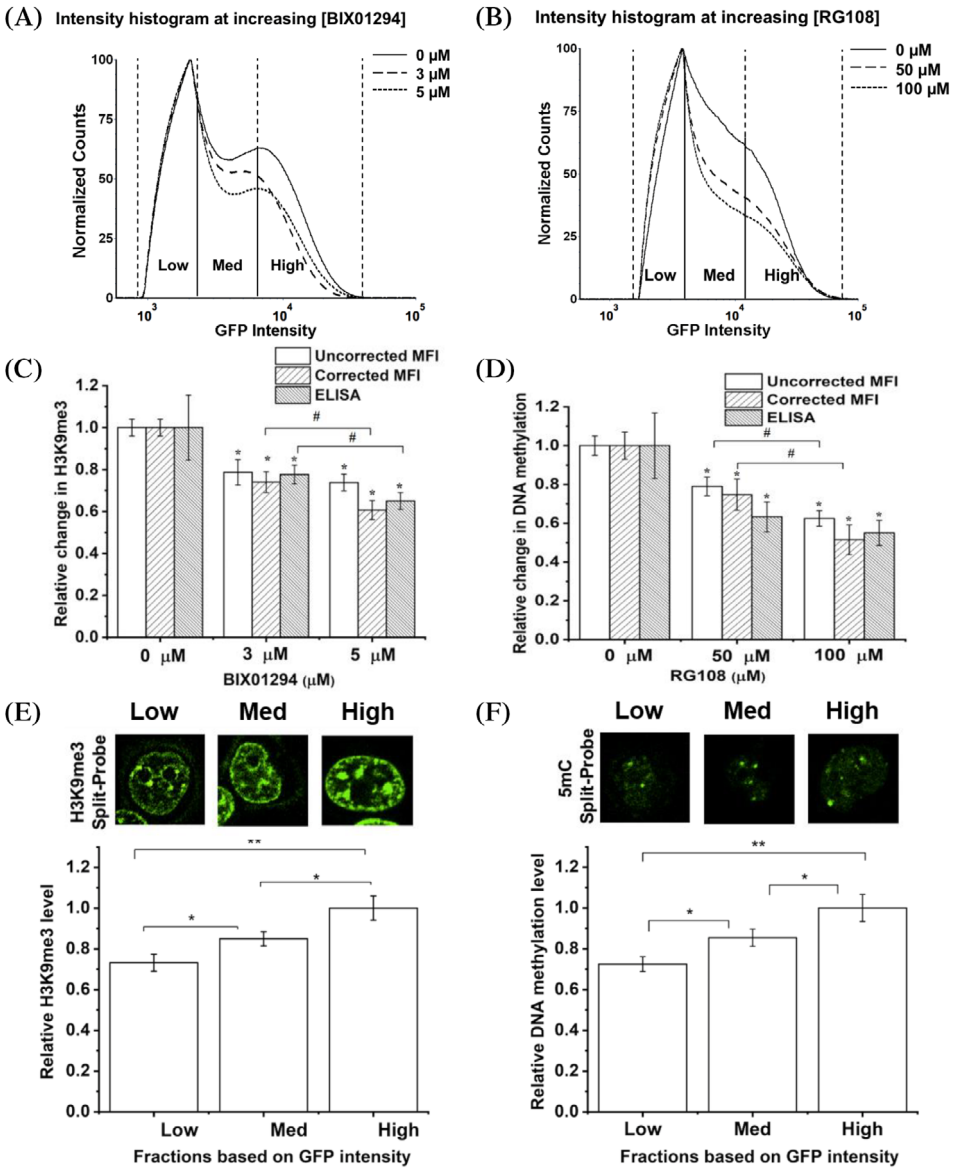

FIGURE 3 Representative flow cytometry histograms of HEK293T cells transfected with (A) H3K9me3 and (B) 5mC probe pairs treated with varying concentrations of epigenetic inhibitors. The measured and corrected MFI determined from such histograms are summarized in (C) and (D) for H3K9me3 and 5mC, respectively. Relative changes in the corresponding epigenetic modification were also determined using ELISA. Relative changes were compared against the untreated group (*) or within drug treatment groups (#) with the same measurement (MFI or ELISA). HEK293T cells were then sorted into subpopulations with different intensity as indicated by vertical lines in (A) and (B). The relative epigenetic levels (normalized to high bin) in each subpopulation is determined using ELISA for cells sorted using (E) H3K9me3 and (F) 5mC BiFC probes. Data is representative of $n = 3$ biologically independent repeats for the ELISA and FACS samples, error bars indicate standard deviation. * Represents $p < 0.05$ and ** represents $p < 0.01$ from a one-way ANOVA followed by Tukey's post hoc test. Images are 2D confocal slices of cells [Color figure can be viewed at wileyonlinelibrary.com]

via ELISA in Figure 3C and D for cell transfected with H3K9me3 and 5mC split-probes, respectively. To account for the effect of epigenetic drugs in the expression of fluorescent proteins, a control experiment was performed using a plasmid containing NLS fused to EGFP. Changes in intensity histogram and MFI are reported in Figure S8 (Supporting Information). The selected epigenetic inhibitors can slightly perturb the expression of fluorescent proteins. The relative changes in expression levels were thus used as a correcting factor for MFI and reported as corrected MFI in Figure 3C and D.

Upon BIX01294 treatment, the normalized intensity histogram shows decreased number of cells in Medium and High intensity bin (Figure 3A), suggesting the loss of highly fluorescent species corresponding to cells with high H3K9me3 levels consistent with our findings in Figure 2E. The values of measured and corrected MFI both decrease with increasing drug concentrations with relative changes in the values of corrected MFI closely resembling relative changes in H3K9me3 levels determined via ELISA, suggesting MFI as a viable measurement to quantify epigenetic changes in live cells.

Treating cells with RG108 gives rise to distinctive intensity histograms as shown in Figure 3B. Noteworthily, the shape of the histogram is quite different from that observed for cells transfected with H3K9me3 split-probes. Higher RG108 concentrations result in the diminishing of high fluorescent intensity peaks in the histograms. Changes in MFI correlates well with changes in 5mC levels as determined via ELISA (Figure 3D). Combined with results above, our engineered split-probes can be applied in FACS to capture quantitative changes in epigenetic modification levels.

To account for the observed histogram of probes and potentially relate that to epigenome heterogeneity within cells, we sorted cells (transfected but untreated) into distinctive sub-populations based on fluorescence intensity. Three sub-populations, namely, Low, Medium, and High were defined based on fluorescence intensities (vertical lines on the intensity histograms in Figure 3A and B identify the gates for binning the cells). Sorted cells were analyzed right away to reveal their epigenetic modification level via ELISA as shown in Figure 3E and F; and can also be reseeded into a culture dish for continuous monitoring

as shown in Figure 3E and F (top). These cells are viable after sorting and can continuously divide. Reseeded cells exhibit the expected fluorescent intensity variations and maintain these characteristics for ~48 h post-sorting. Significant epigenetic changes were observed among sorted subpopulations (Figure 3E,F). Specifically, the High species sorted based on H3K9me3 split-probe exhibited ~25% increase in H3K9me3 levels compared to the Low species, and about a 19% higher compared to the Medium species. Similar observations were made in cell populations sorted via the intensity of 5mC split-probes (Figure 3F). Although the observed fluorescence intensity changes may have contributions from difference in transfection efficiency of split-probes (the effects of transfection efficiency were partially teased out using corrected MFI), the changes in 5mC and H3K9me3 levels are expected to play a significant role as demonstrated in our ELISA results.

Collectively, we have identified that split-based epigenetic probes can offer quantitative accuracy in gauging the epigenetic distribution among cell populations and enable cell sorting based on epigenetic modification level. Compared to microscopy-based analysis, FACS can easily analyze thousands of cells in hours and thus more truthfully reveal the distribution of split-probe intensity among cell population. Furthermore, the ability to sort cells into different intensity bins with distinctive epigenetic modification levels enable us to evaluate how epigenome affect drug resistance and tumor evolution in breast cancer cell lines.

3.3 | Distinct epigenetic contributions to tumor heterogeneity in breast cancer cells

Epigenetic modifications are heavily linked with tumor heterogeneity in almost all types of cancers and eventually contribute to differences in drug resistance [61, 62] and tumor evolution [63, 64]. Limited tools exist for profiling the epigenome or for sorting cells based on their epigenetic background to further our understanding of tumor heterogeneity [9]. We thus applied the probes developed in this work toward sorting and analyzing cancer cells for their potential drug resistance and ability to form tumors.

A widely known example of drug resistance is the application of anthracycline drugs, (e.g., doxorubicin) in breast cancer treatments [65, 66]. Drug resistance to doxorubicin can develop in many patients of breast cancer, leading to persistence of tumors or cancer relapse. Several mechanisms are implicated in the development of resistance, including epigenetic factors such as DNA methylation and histone modifications. For instance, the doxorubicin resistant version of the breast cancer cell line MCF7, is characterized by global DNA hypomethylation [42, 67] and the hypomethylation and hypermethylation at specific gene promoters [43].

We can successfully sort MCF7 cells into different subpopulations with varying epigenetic modification level as demonstrated in the previous section. These subpopulations are expected to consist of a uniform genetic background but are heterogeneous in epigenome. The sorted cell subpopulations were then seeded onto Matrigel to assess their respective abilities in forming tumor spheroids. Tumor spheroids were imaged 2 weeks after culture and their size were measured as shown in Figure 4A,B (see also Figure S9 (Supporting Information)). Cell subpopulations containing higher levels of H3K9me3 gave rise to smaller tumor spheroids, indicating slower proliferation activities as shown in Figure 4A. Similar trend was observed in MCF7 cells sorted by 5mC levels as shown in Figure 4B. The probability distribution of tumor spheroid size among the three subpopulations, namely Low, Medium, and High, based on the epigenetic background, resembles each other within each split-probe. It is noticed that the subpopulation with high H3K9me3 level has a higher probability density than the Low or Medium subpopulation particularly below 1250. A similar trend is observed for 5mC for spheroids less than 1000. Collectively, these findings suggest that cells with higher H3K9me3 or 5mC levels seem to preferentially form smaller spheroids with narrower size distributions as compared to spheroids formed using cells with Low or Medium H3K9me3 or 5mC levels. One potential complication in interpreting our results arises from the concern that the presence of probes may perturb or compete with other biological factors in accessing epigenetic markers. Since all probes were introduced to MCF7 via a transient transfection which are expected to last <2 days after the completion of sorting, we do not expect the presence of such probes to significantly impede the normal biological processes that require access to H3K9me3 or 5mC marks during the spheroid growth which takes ~2 weeks. The observed changes in spheroid size are thus likely to originate from difference in epigenetic modification levels in MCF7. The smaller spheroid and slow proliferation features observed in MCF7 with higher level of H3K9me3 and 5mC are consistent with their roles as repressive markers for potentially suppressing proliferation related genes [68, 69]. Higher DNA methylation level in promoter and CpG island is a hallmark of cancer [70]. These methylation regions were reported to be enriched in cell cycle regulating genes, such as $p16^{INK4a}$ [71] which can potentially result in slow cell growth and subsequently smaller spheroid size. Prior literature has shown that inhibition of DNA methylation in MCF7 cells can result in higher proliferation rate which is consistent with our findings [72]. There is, however, only scarce information regarding the role of H3K9me3 on the regulation of breast cancer progression hindering a direct comparison from this work.

We then tested these subpopulations for their response to doxorubicin. As a benchmark experiment, we determined the IC50 of doxorubicin for unsorted MCF7 to be ~0.9 μM as shown in Figure S10 (Supporting Information). Sorted cell subpopulations were then treated to 0.5 and 1 μM of doxorubicin for 48 h to determine their respective responses under these two selected concentrations. The viability of sorted cells is measured via an MTT assay with results summarized in Figure 4C,D. No appreciable differences in cell viability were noticed at a doxorubicin concentration of 0.5 μM. At the higher exposure dose, however, the cell viability differs significantly for subpopulations sorted based on H3K9me3 or 5mC. Specifically, MCF7 cells with higher H3K9me3 levels exhibits reduced cytotoxicity suggesting reduced sensitivity toward doxorubicin. MCF7 cells with

higher 5mC level, on the other hand, seems to be more responsive to doxorubicin treatment. Global DNA hypomethylation was observed in MCF7 cells resistant to doxorubicin based on previous literature [43, 67] which is consistent with our observations predicting high drug responsiveness in cells with a high 5mC level. The effects of histone methylation on cancer drug resistance are less well understood. A prior study of MCF7 treated with doxorubicin found no significant changes in H3K9me3 [42]. Other studies have treated different cancer cell lines, such as breast (SkBr3) and lung (A549) cells, with doxorubicin and found increase in H3K9me3 levels compared to their parental line [73] aligning with our observations. Furthermore, several chemo-drugs were shown to induce reductions in H3K9me3 leading

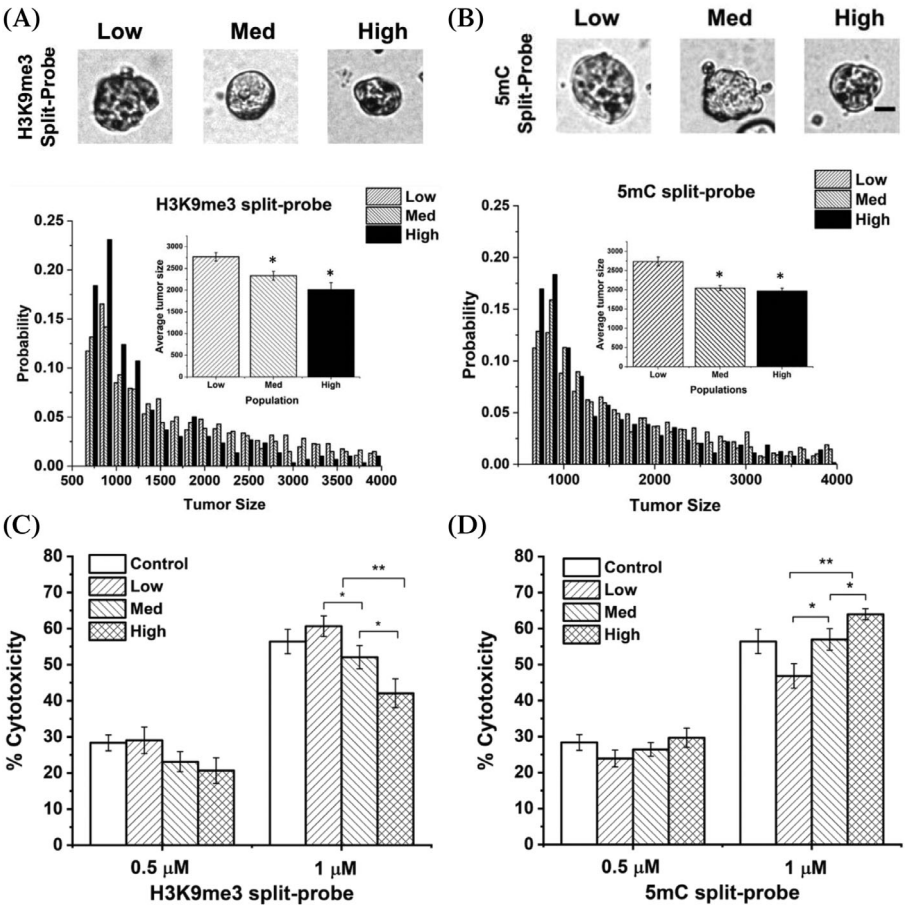

FIGURE 4 Sorted MCF7 cells based on different levels of (A) H3K9me3 and (B) 5mC form tumor spheroids of different sizes on Matrigel coated surface. Top: Representative images of tumor spheroids. Scale bar = 25 μm. Bottom: Histogram of tumor spheroid size grown from sorted MCF7 cells based on the epigenetic level indicated by split-probe intensity. Inset: Bar plots compared tumor spheroid seeded using sorted cell subpopulations with distinctive epigenetic level (*$p < 0.05$ compared to low via t-test). The percentage of cytotoxicity of cells responding to doxorubicin treatment with varying (C) H3K9me3 and (D) 5mC levels. The % cytotoxicity was determined via an MTT assay. Data = mean ± S.E., $n = 3$ biologically independent repeats.
* Indicates statistically significant differences from a one-way ANOVA following by a post-hoc Tukey test ($p = 0.05$)

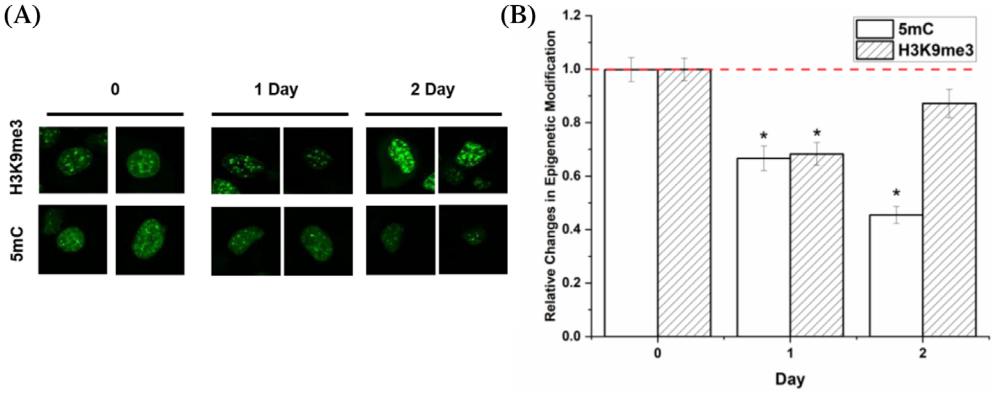

FIGURE 5 (A) Representative images of MCF7 cells transfected with H3K9me3 and 5mC split-probes and treated with 1 μM of doxorubicin. Images are 2D projections of confocal Z-stacks. (B) Relative changes in 5mC (open) and H3K9me3 (shaded) after treating with1 μM Dox for different durations. Relative changes in epigenetic modifications are reported as relative intensity changes in split-probes normalized to split-probe intensity without Dox treatment at the same timepoint. Data = mean ± S.E. *$p < 0.05$ (one-way ANOVA followed by a post-hoc Tukey test). $n = 6$, biological replicates [Color figure can be viewed at wileyonlinelibrary.com]

to apoptosis [74, 75] providing a plausible foundation for high cytotoxicity in cell populations with low H3K9me3 level.

To verify the antagonistic effects observed for H3K9me3 and 5mC, we transfected MCF7 cells with our split-probes and tracked changes in epigenome by continuous treatment with doxorubicin. Typical images of cells under treatments are shown in Figure 5A. After treatment, surviving cells exhibit significantly lower 5mC levels. Interestingly, cellular H3K9me3 levels decrease initially but start to come back with time suggesting its involvement in a potential adaptation mechanism. To account for expression level changes from day-to-day, we also tracked transfected MCF7 cells in absence of doxorubicin as shown in Figure S11 (Supporting Information). Relative changes in H3K9me3 and 5mC with time, corrected by day-to-day variations, are summarized in Figure 5B consistent with our visual observations.

Collectively, our results suggest that an epigenetic mechanism is involved in the acquisition of drug resistance. Cells with higher H3K9me3 levels are likely to survive the treatment of doxorubicin while cells with higher 5mC is more likely to respond and result in cell death. Live cell treatment experiment also validates our finding that surviving cells exhibit lower degree of global DNA methylation levels. Numerous studies have highlighted similar findings [43, 67, 76] in doxorubicin resistant versions of MCF7, showing global DNA hypomethylation in these cells. The underlying connection between histone methylation and Doxorubicin resistance in breast cancer cells is still poorly understood. There is some evidence from acute leukemia cells suggesting that certain histone modifications (including H3K9me3) are enriched in doxorubicin resistant versions of the leukemia cells [77]. Similar observations were also made in induced multidrug-tolerant melanoma cells [78]. One antibody based analysis of histone modification levels of a doxorubicin resistant version of MCF7 potentially indicates the H3K9me3 levels between the two versions are not significantly altered [43]. Our data, however, unequivocally suggests that elevated levels of H3K9me3 might be linked to development of doxorubicin resistance in MCF7 cells.

4 | CONCLUSIONS

In this work, we developed a platform technology to analyze and sort single cells based on their epigenetic modification levels, specifically H3K9me3 and 5mC. Cells can be analyzed using FACS to reveal their intrinsic heterogeneity in epigenetic modifications. The sorting capability developed by our novel sensors allows us to unequivocally dissect epigenetic contributions to tumor spheroid growth and the development of drug resistance. Using breast cancer cell line MCF7 as a model system, our results suggest that MCF7 cells with higher H3K9me3 levels are more likely to be develop resistance to Doxorubicin, while an opposite trend was observed for 5mC.

ACKNOWLEDGMENTS

We would like to thank Dr. Jill Hutchcroft at the Purdue Flow Cytometry Facility for her help with sorting the cells on the BD FACS Aria III cell sorter and Gregory Cresswell with his help in using the BD FACS Aria. The MCF7 cell lines were a kind gift from Dr. Sophie Lelievre's lab. This work was supported by National Science Foundation (CBET-1512285, CBET-1705560, & EF-1935226), and Indiana Clinical and Translational Science Institute. The authors also gratefully acknowledge the support from the Purdue University Center for Cancer Research, NIH grant P30 CA023168.

AUTHOR CONTRIBUTIONS

Agnes Mendonca: Conceptualization (equal); data curation (equal); formal analysis (equal); methodology (equal); visualization (equal); writing – original draft (equal). **Oscar Sanchez:** Conceptualization (equal); data curation (equal); investigation (equal); methodology (equal); visualization (equal); writing – original draft (equal); writing – review and editing (equal). **Han Zhao:** Data curation (equal); methodology (equal); validation (equal); writing – review and editing (equal). **Li Lin:** Investigation (equal); methodology (equal); writing – review and editing (equal). **Alan Min:** Data curation (equal); formal analysis (equal); methodology (equal); writing – review and editing (equal). **Chongli Yuan:** Conceptualization (equal); funding acquisition (equal); resources (equal); writing – original draft (equal); writing – review and editing (equal).

CONFLICT OF INTEREST

The authors declare no competing interests.

PEER REVIEW

The peer review history for this article is available at https://publons.com/publon/10.1002/cyto.a.24530.

ORCID

Chongli Yuan https://orcid.org/0000-0003-3765-0931

REFERENCES

1. Ehrlich M, Gama-Sosa MA, Huang L-H, Midgett RM, Kuo KC, McCune RA, et al. Amount and distribution of 5-methylcytosine in human DNA from different types of tissues or cells. Nucleic Acids Res. 1982;10:2709–21.
2. Razin A, Cedar H. DNA methylation and genomic imprinting. Cell. 1994;77:473–6.
3. Lippman Z, Gendrel A-V, Black M, Vaughn MW, Dedhia N, McCombie WR, et al. Role of transposable elements in heterochromatin and epigenetic control. Nature. 2004;430:471–6.
4. Becker JS, Nicetto D, Zaret KS. H3K9me3-dependent heterochromatin: barrier to cell fate changes. Trends Genet. 2016;32:29–41.
5. Mikkelsen TS, Ku M, Jaffe DB, Issac B, Lieberman E, Giannoukos G, et al. Genome-wide maps of chromatin state in pluripotent and lineage-committed cells. Nature. 2007;448:553–60.
6. Kulis M, Esteller M. DNA methylation and cancer. Advances in Genetics. Volume 70. San Diego, CA: Academic Press; 2010. p. 27–56.
7. Leszinski G, Gezer U, Siegele B, Stoetzer O, Holdenrieder S. Relevance of histone marks H3K9me3 and H4K20me3 in cancer. Anticancer Res. 2012;32:2199–205.
8. Rosenthal R, McGranahan N, Herrero J, Swanton C. Deciphering genetic intratumor heterogeneity and its impact on cancer evolution. Annu Rev Cancer Biol. 2017;1:223–40.
9. Mazor T, Pankov A, Song JS, Costello JF. Intratumoral heterogeneity of the epigenome. Cancer Cell. 2016;29:440–51.
10. Balko JM, Cook RS, Vaught DB, Kuba MG, Miller TW, Bhola NE, et al. Profiling of residual breast cancers after neoadjuvant chemotherapy identifies DUSP4 deficiency as a mechanism of drug resistance. Nat Med. 2012;18:1052–9.

11. Gifford G, Paul J, Vasey PA, Kaye SB, Brown R. The acquisition of hMLH1 methylation in plasma DNA after chemotherapy predicts poor survival for ovarian cancer patients. Clin Cancer Res. 2004;10: 4420–6.
12. Holohan C, Van Schaeybroeck S, Longley DB, Johnston PG. Cancer drug resistance: an evolving paradigm. Nat Rev Cancer. 2013;13: 714–26.
13. Zeller C, Dai W, Steele NL, Siddiq A, Walley AJ, Wilhelm-Benartzi C, et al. Candidate DNA methylation drivers of acquired cisplatin resistance in ovarian cancer identified by methylome and expression profiling. Oncogene. 2012;31:4567–76.
14. Çelik-Uzuner S, Li Y, Peters L, O'Neill C. Measurement of global DNA methylation levels by flow cytometry in mouse fibroblasts. In Vitro Cell Dev Biol-Anim. 2017;53:1–6.
15. Desjobert C, El Mai M, Gérard-Hirne T, Guianvarc'h D, Carrier A, Pottier C, et al. Combined analysis of DNA methylation and cell cycle in cancer cells. Epigenetics. 2015;10:82–91.
16. Watson M, Chow S, Barsyte D, Arrowsmith C, Shankey TV, Minden M, et al. The study of epigenetic mechanisms based on the analysis of histone modification patterns by flow cytoametry. Cytometry A. 2014;85:78–87.
17. Obier N, Müller AM. Chromatin flow cytometry identifies changes in epigenetic cell states. Cells Tissues Organs. 2010;191:167–74.
18. Hayashi-Takanaka Y, Yamagata K, Wakayama T, Stasevich TJ, Kainuma T, Tsurimoto T, et al. Tracking epigenetic histone modifications in single cells using fab-based live endogenous modification labeling. Nucleic Acids Res. 2011;39:6475–88.
19. Sato Y, Mukai M, Ueda J, Muraki M, Stasevich TJ, Horikoshi N, et al. Genetically encoded system to track histone modification in vivo. Sci Rep. 2013;3:2436.
20. A. M.-F. Delachat, N. Guidotti, A. L. Bachmann, A. C. Meireles-Filho, H. Pick, C. C. Lechner, et al., "Engineered multivalent sensors to detect coexisting histone modifications in living stem cells," Cell Chem Biol, vol. 25, pp. 51–56. e6, 2018.
21. Sanchez OF, Mendonca A, Carneiro AD, Yuan C. Engineering recombinant protein sensors for quantifying histone acetylation. ACS Sensors. 2017;2:426–35.
22. Sánchez OF, Mendonca A, Min A, Liu J, Yuan C. Monitoring histone methylation (H3K9me3) changes in live cells. ACS Omega. 2019;4: 13250–9.
23. Sasaki K, Yoshida M. Genetically encoded FRET indicators for live-cell imaging of histone acetylation. Fluorescent protein-based biosensors. Methods in Molecular Biology. Vol. 1071, Totowa, NJ: Humana Press; 2014. p. 151–61.
24. Lungu C, Pinter S, Broche J, Rathert P, Jeltsch A. Modular fluorescence complementation sensors for live cell detection of epigenetic signals at endogenous genomic sites. Nat Commun. 2017;8:1–13.
25. Sato Y, Kujirai T, Arai R, Asakawa H, Ohtsuki C, Horikoshi N, et al. A genetically encoded probe for live-cell imaging of H4K20 monomethylation. J Mol Biol. 2016;428:3885–902.
26. Ueda J, Maehara K, Mashiko D, Ichinose T, Yao T, Hori M, et al. Heterochromatin dynamics during the differentiation process revealed by the DNA methylation reporter mouse, MethylRO. Stem Cell Rep. 2014;2:910–24.
27. Jørgensen HF, Adie K, Chaubert P, Bird AP. Engineering a high-affinity methyl-CpG-binding protein. Nucleic Acids Res. 2006;34: e96–6.
28. Peng Q, Lu S, Shi Y, Pan Y, Limsakul P, Chernov AV, et al. Coordinated histone modifications and chromatin reorganization in a single cell revealed by FRET biosensors. Proc Natl Acad Sci. 2018;115: E11681–90.
29. Lin C-W, Jao CY, Ting AY. Genetically encoded fluorescent reporters of histone methylation in living cells. J Am Chem Soc. 2004;126: 5982–3.
30. Ito T, Umehara T, Sasaki K, Nakamura Y, Nishino N, Terada T, et al. Real-time imaging of histone H4K12–specific acetylation determines the modes of action of histone deacetylase and bromodomain inhibitors. Chem Biol. 2011;18:495–507.
31. Sasaki K, Ito T, Nishino N, Khochbin S, Yoshida M. Real-time imaging of histone H4 hyperacetylation in living cells. Proc Natl Acad Sci. 2009;106:16257–62.
32. Tekel SJ, Vargas DA, Song L, LaBaer J, Caplan MR, Haynes KA. Tandem histone-binding domains enhance the activity of a synthetic chromatin effector. ACS Synth Biol. 2018;7:842–52.
33. Albanese KI, Krone MW, Petell CJ, Parker MM, Strahl BD, Brustad EM, et al. Engineered reader proteins for enhanced detection of methylated lysine on histones. ACS Chem Biol. 2019;15:103–11.
34. Bannister AJ, Zegerman P, Partridge JF, Miska EA, Thomas JO, Allshire RC, et al. Selective recognition of methylated lysine 9 on histone H3 by the HP1 chromo domain. Nature. 2001;410:120–4.
35. Fischle W, Franz H, Jacobs SA, Allis CD, Khorasanizadeh S. Specificity of the chromodomain Y chromosome family of chromodomains for lysine-methylated ARK (S/T) motifs. J Biol Chem. 2008;283: 19626–35.
36. Dong C, Liu Y, Lyu T-J, Beldar S, Lamb KN, Tempel W, et al. Structural basis for the binding selectivity of human CDY chromodomains. Cell Chem Biol. 2020;27:827–838. e7.
37. Fischle W, Tseng BS, Dormann HL, Ueberheide BM, Garcia BA, Shabanowitz J, et al. Regulation of HP1–chromatin binding by histone H3 methylation and phosphorylation. Nature. 2005;438:1116–22.
38. Du Q, Luu P-L, Stirzaker C, Clark SJ. Methyl-CpG-binding domain proteins: readers of the epigenome. Epigenomics. 2015;7:1051–73.
39. Jeltsch A, Broche J, Lungu C, Bashtrykov P. Biotechnological applications of MBD domain proteins for DNA methylation analysis. J Mol Biol. 2020;432:1816–23.
40. Yamagata K. DNA methylation profiling using live-cell imaging. Methods. 2010;52:259–66.
41. Yuan J, Xu WW, Jiang S, Yu H, Poon HF. The scattered twelve tribes of HEK293. Biomed Pharmacol J. 2018;11:621–3.
42. Vasyl'F C, Lukyanova NY, Kovalchuk O, Tryndyak VP, Pogribny IP. Epigenetic profiling of multidrug-resistant human MCF-7 breast adenocarcinoma cells reveals novel hyper-and hypomethylated targets. Mol Cancer Ther. 2007;6:1089–98.
43. Chekhun VF, Kulik GI, Yurchenko OV, Tryndyak VP, Todor IN, Luniv LS, et al. Role of DNA hypomethylation in the development of the resistance to doxorubicin in human MCF-7 breast adenocarcinoma cells. Cancer Lett. 2006;231:87–93.
44. Phelan K, May KM. Basic techniques in mammalian cell tissue culture. Curr Protoc Cell Biol. 2015;66:1.1.1–1.1.22.
45. Kubicek S, O'Sullivan RJ, August EM, Hickey ER, Zhang Q, Teodoro ML, et al. Reversal of H3K9me2 by a small-molecule inhibitor for the G9a histone methyltransferase. Mol Cell. 2007;25: 473–81.
46. Brueckner B, Boy RG, Siedlecki P, Musch T, Kliem HC, Zielenkiewicz P, et al. Epigenetic reactivation of tumor suppressor genes by a novel small-molecule inhibitor of human DNA methyltransferases. Cancer Res. 2005;65:6305–11.
47. Savickiene J, Treigyte G, Jazdauskaite A, Borutinskaite VV, Navakauskiene R. DNA methyltransferase inhibitor RG108 and histone deacetylase inhibitors cooperate to enhance NB4 cell differentiation and E-cadherin re-expression by chromatin remodelling. Cell Biol Int. 2012;36:1067–78.
48. Lin LF, Xie J, Sánchez OF, Bryan C, Freeman JL, Yuan C. Low dose lead exposure induces alterations on heterochromatin hallmarks persisting through SH-SY5Y cell differentiation. Chemosphere. 2021; 264:128486.
49. Goldstein M, Watkins S. Immunohistochemistry. Curr Protoc Mol Biol. 2008;81:14.6.1–14.6.23.

50. Beaujean N, Salvaing J, Abd Hadi NA, Pennings S. Antibody-based detection of global nuclear DNA methylation in cells, tissue sections, and mammalian embryos. DNA Methylation Protocols. Methods in Molecular Biology, Vol. 1708. New York, NY: Humana Press; 2018. p. 59–80.
51. Kim S-E, Chang M, Yuan C. One-pot approach for examining the DNA methylation patterns using an engineered methyl-probe. Biosens Bioelectron. 2014;58:333–7.
52. Ohki I, Shimotake N, Fujita N, Jee J-G, Ikegami T, Nakao M, et al. Solution structure of the methyl-CpG binding domain of human MBD1 in complex with methylated DNA. Cell. 2001;105:487–97.
53. Mendonca A, Sánchez OF, Xie J, Carneiro A, Lin L, Yuan C. Identifying distinct heterochromatin regions using combinatorial epigenetic probes in live cells. Biochim Biophys Acta – Gene Regul Mech. 2021; 1864:194725.
54. Politz JCR, Scalzo D, Groudine M. Something silent this way forms: the functional organization of the repressive nuclear compartment. Annu Rev Cell Dev Biol. 2013;29:241–70.
55. Hori Y, Norinobu T, Sato M, Arita K, Shirakawa M, Kikuchi K. Development of fluorogenic probes for quick no-wash live-cell imaging of intracellular proteins. J Am Chem Soc. 2013;135:12360–5.
56. Sánchez OF, Lin L, Bryan CJ, Xie J, Freeman JL, Yuan C. Profiling epigenetic changes in human cell line induced by atrazine exposure. Environ Pollut. 2020;258:113712.
57. Chang Y, Zhang X, Horton JR, Upadhyay AK, Spannhoff A, Liu J, et al. Structural basis for G9a-like protein lysine methyltransferase inhibition by BIX-01294. Nat Struct Mol Biol. 2009;16:312–7.
58. Thiemann RF, Nelson DA, DiPersio CM, Larsen M, LaFlamme SE. Establishment of a murine pro-acinar cell line to characterize roles for FGF2 and α3β1 integrins in regulating pro-acinar characteristics. Sci Rep. 2019;9:1–12.
59. Kodama Y, Hu C-D. Bimolecular fluorescence complementation (BiFC): a 5-year update and future perspectives. Biotechniques. 2012; 53:285–98.
60. Shyu YJ, Hu C-D. Fluorescence complementation: an emerging tool for biological research. Trends Biotechnol. 2008;26:622–30.
61. Brown R, Glasspool R. Epigenetic modulation of resistance to chemotherapy? Ann Oncol. 2007;18:1429–30.
62. Glasspool R, Teodoridis JM, Brown R. Epigenetics as a mechanism driving polygenic clinical drug resistance. Br J Cancer. 2006;94: 1087–92.
63. Baylin SB, Herman JG. DNA hypermethylation in tumorigenesis: epigenetics joins genetics. Trends Genet. 2000;16:168–74.
64. Easwaran H, Tsai H-C, Baylin SB. Cancer epigenetics: tumor heterogeneity, plasticity of stem-like states, and drug resistance. Mol Cell. 2014;54:716–27.
65. Dean-Colomb W, Esteva FJ. Emerging agents in the treatment of anthracycline-and taxane-refractory metastatic breast cancer. Semin Oncol; 2008;35:S31–S38.
66. Fornari FA, Randolph JK, Yalowich JC, Ritke MK, Gewirtz DA. Interference by doxorubicin with DNA unwinding in MCF-7 breast tumor cells. Mol Pharmacol. 1994;45:649–56.
67. Luzhna L, Kovalchuk O. Modulation of DNA methylation levels sensitizes doxorubicin-resistant breast adenocarcinoma cells to radiation-induced apoptosis. Biochem Biophys Res Commun. 2010;392:113–7.
68. Sha J, Han Q, Chi C, Zhu Y, Pan J, Dong B, et al. Upregulated KDM4B promotes prostate cancer cell proliferation by activating autophagy. J Cell Physiol. 2020;235:2129–38.
69. Poloni A, Maurizi G, Mattiucci D, Amatori S, Fogliardi B, Costantini B, et al. Overexpression of CDKN2B (p15INK4B) and altered global DNA methylation status in mesenchymal stem cells of high-risk myelodysplastic syndromes. Leukemia. 2014;28:2241–4.
70. Sproul D, Meehan RR. Genomic insights into cancer-associated aberrant CpG Island hypermethylation. Brief Funct Genomics. 2013;12: 174–90.
71. Das PM, Singal R. DNA methylation and cancer. J Clin Oncol. 2004; 22:4632–42.
72. Ateeq B, Unterberger A, Szyf M, Rabbani SA. Pharmacological inhibition of DNA methylation induces proinvasive and prometastatic genes in vitro and in vivo. Neoplasia. 2008;10:266–78.
73. Al Emran A, Marzese DM, Menon DR, Stark MS, Torrano J, Hammerlindl H, et al. Distinct histone modifications denote early stress-induced drug tolerance in cancer. Oncotarget. 2018;9: 8206–22.
74. Lee J-K, Kim K-C. DZNep, inhibitor of S-adenosylhomocysteine hydrolase, down-regulates expression of SETDB1 H3K9me3 HMTase in human lung cancer cells. Biochem Biophys Res Commun. 2013; 438:647–52.
75. Tabata K, Sakai H, Nakajima R, Saya-Nishimura R, Motani K, Okano S, et al. Acute application of cisplatin affects methylation status in neuroblastoma cells. Oncol Rep. 2011;25:1655–60.
76. Boettcher M, Kischkel F, Hoheisel JD. High-definition DNA methylation profiles from breast and ovarian carcinoma cell lines with differing doxorubicin resistance. PLoS One. 2010;5:e11002.
77. Liu T, Guo Q, Guo H, Hou S, Li J, Wang H. Quantitative analysis of histone H3 and H4 post-translational modifications in doxorubicin-resistant leukemia cells. Biomed Chromatogr. 2016;30:638–44.
78. Ravindran Menon D, Das S, Krepler C, Vultur A, Rinner B, Schauer S, et al. A stress-induced early innate response causes multidrug tolerance in melanoma. Oncogene. 2015;34:4448–59.

SUPPORTING INFORMATION

Additional supporting information may be found in the online version of the article at the publisher's website.

How to cite this article: Mendonca A, Sánchez O, Zhao H, Lin L, Min A, Yuan C. Development and application of novel BiFC probes for cell sorting based on epigenetic modification. Cytometry. 2022;101:339–50. https://doi.org/10.1002/cyto.a.24530